Propulsion and Power Research 2014;3(4):175–186

HOSTED BY

ELSEVIER

http://ppr.buaa.edu.cn/

Propulsion and Power Research

www.sciencedirect.com

Numerical simulations of single and multi-staged injection of H_2 in a supersonic scramjet combustor

L. Abu-Farah*, O.J. Haidn, H.-P. Kau

Institute of Flight Propulsion, Technische Universitaet Muenchen, Boltzmannstrasse 15, D-85748 Garching bei Muenchen, Germany

Received 5 May 2014; accepted 3 November 2014
Available online 3 January 2015

KEYWORDS

Computational fluid dynamics (CFD)
Reynolds-averaged Navier-stokes (RANS) simulation;
Supersonic combustor;
Shear stress transport (SST) k-ω;
Static pressures;
H_2/air mixing;
Single/multi-stage injection

Abstract Computational fluid dynamics (CFD) simulations of a single staged injection of H_2 through a central wedge shaped strut and a multi-staged injection through wall injectors are carried out by using Ansys CFX-12 code. Unstructured tetrahedral grids for narrow channel and quarter geometries of the combustor are generated by using ICEM CFD. Steady three-dimensional (3D) Reynolds-averaged Navier-stokes (RANS) simulations are carried out in the case of no H_2 injection and compared with the simulations of single staged pilot and/or main H_2 injections and multistage injection. Shear stress transport (SST) based on k-ω turbulent model is adopted. Flow field visualization (complex shock waves interactions) and static pressure distribution along the wall of the combustor are predicted and compared with the experimental schlieren images and measured wall static pressures for validation. A good agreement is found between the CFD predicted results and the measured data. The narrow and quarter geometries of the combustor give similar results with very small differences. Multi-staged injections of H_2 enhance the turbulent H_2/air mixing by forming vortices and additional shock waves (bow shocks).

1. Introduction

The supersonic combustor ramjet (Scramjet) allows the flow through the engine to remain supersonic. The scramjet engine is the most promising air breathing propulsive system and appropriate choice for hypersonic flight ($Ma > 5$). Many researchers are working on the development of the scramjet engine due to its applications in the military missiles, low cost space access, and space tourism in particular [1].

Supersonic combustion is a challenging, complex process which includes many phenomena such as turbulent mixing between air and H_2, shock generation and interaction, heat release, and the reaction products' flow field which is

*Corresponding author. Tel.: +49 1741089719.
E-mail address: lailaabufarah@yahoo.com (L. Abu-Farah).

Peer review under responsibility of National Laboratory for Aeronautics and Astronautics, China.

2212-540X © 2015 National Laboratory for Aeronautics and Astronautics. Production and hosting by Elsevier B.V. All rights reserved.
http://dx.doi.org/10.1016/j.jppr.2014.12.001

affected by the combustor geometry [2]. To achieve efficient combustion, it is necessary to enhance and accelerate the mixing between the fuel and the air as well as to reduce the pressure losses in the combustion [3]. The flow field within the combustor of the scramjet engine is very complex and has a tremendous impact on the optimum supersonic combustor design. Sufficient mixing to the extent that the desired combustion reaction and heat release can occur requires a detailed understanding of fuel injection and fluid interaction processes [4].

Efficient mixing is an important aspect in reducing skin friction drag and maintaining short combustor length. Due to rapid fuel/air mixing in supersonic flows and short air residence time, efficient mixing is hard to achieve with the given requirement of minimum pressure losses in the total pressure. Low mixing rates are obtained due to the compressibility effects at high convective Mach numbers.

Eddy generation can prolong the residence time of the mixture in the supersonic flow [5]. Mixing enhancement can be achieved through the use of shock waves or the creation of stream wise vorticity that is affected by strut geometry [6–8]. Shigeru Aso et al. [9] found that the shock generator is an effective method to accelerate the combustion, where increasing the injection total pressure raises the penetration of fuel and thus the reaction zone expands to the centre of the flow field.

Computational analysis for single and multi-staged injection of H_2 is done in this research work for better understanding of the H_2/air mixing. First staged injection through the central strut in the pilot ports – parallel to the flow direction – and in the main ports – perpendicular to the main flow – increases the penetration depth of H_2 in air. Wall injectors, normal to the main flow, are used to exploit the unburned oxygen close to the upper and lower walls of the combustor. This is done because the hydrogen injected through the first stage does not penetrate the entire cross sectional area of the combustor and to reduce the risk of thermal choking in a supersonic combustor in a multi-staged injection. K. Kumaran, V. Babu [10] and P. Gerlinger [5] made numerical studies of mixing and combustion enhancement in supersonic combustors. The effects of multi-staged injection on the supersonic mixing and combustion were studied numerically by Hou Lingyun and Bernhad Weigand [11]. They found that the second staged injection can exploit the residual oxygen near the wall resulting in good burning effects after the wall injection and more heat release.

It is found that transverse injection systems cause a significant blockage of the flow resulting in irreversibilities due to shock waves and thrust losses. In addition, the penetration of the fuel jet may be insufficient. Wall injectors have the advantages of ease in manufacturing, simplicity in cooling, and no pressure losses if switched off in the case of staged injection [12,13].

For efficient combustion, fuel and air should be mixed to approximately stoichiometric proportions [14]. Hence, optimization of this mixing process is the key research topic [5]. With increasing combustor Mach number, the degree of fuel-air mixing that is achieved through the natural convective and diffusive processes is reduced leading to a decrease in combustor efficiency and thrust [15]. Fuel jets and compressible shear layers are characteristic features of any scramjet. Mixing these shear layers are characterized by large scale eddies that form due to the high shear between the fuel and air streams [16]. These eddies entrain the fuel and air into the mixing region between the fluids leading to increased interfacial area and locally steep concentration gradient, thus increasing the importance of the molecular diffusion across the interfaces. The spreading rate of the compressible layers is lower than that for the incompressible layers [17–19]. Using the divergent walls of the combustor can accelerate the flow without the risk of thermal choking.

Most research fields focus on hydrogen-fuelled scramjets as hydrogen is the fuel of choice for high speed flight. This is the result of hydrogen's properties such as high heat of combustion (141.9 kJ/g), high molecular diffusion velocity, and high specific heat, i.e., its cooling capacity. In fact, the cooling capacity is one of the most important properties that strongly influence the fuel selection for high speed flight systems [20].

The aim of this work is to analyse and determine the best H_2 injection and mixing conditions with air through the investigation of the flow pattern, the complex shock waves interactions, boundary layer separations near the combustor walls and the total pressure losses in the combustor. Moreover, the aim is to predict the pressure distribution along the wall of the combustion chamber and to achieve the flow field visualization of H_2/air by computational fluid dynamics (CFD) simulations. To enhance the turbulent H_2/air mixing efficiency, the effects of single and multi-stage injections on the pressure and flow fields are studied and compared with the experimental data for validation.

2. Flow modelling and simulation

2.1. Geometry and grid generation

ICEM CFD 12.1 is used to create the three-dimensional (3D) geometry and grid. Quarter and narrow channel of the combustion chamber are generated. The sizes of the combustion chamber and the main strut injector are similar to those used in the experiment at LFA [21] as can be seen in Figures 1(a) and (b). The combustor consists of two parts. The first one has a constant cross sectional area of 2 mm × 25 mm with a total length of 89 mm. In this section the strut injector is located at a distance of 28 mm from the entrance of the combustor. The wedged strut in the quarter geometry consists of 14 H_2 main injector ports with a diameter of 0.4 mm (red colour), 4 H_2 pilot injectors with a diameter of 0.6 mm (green colour) and 2 Air pilot injectors with a diameter of 0.6 m (blue colour). The wedged strut in

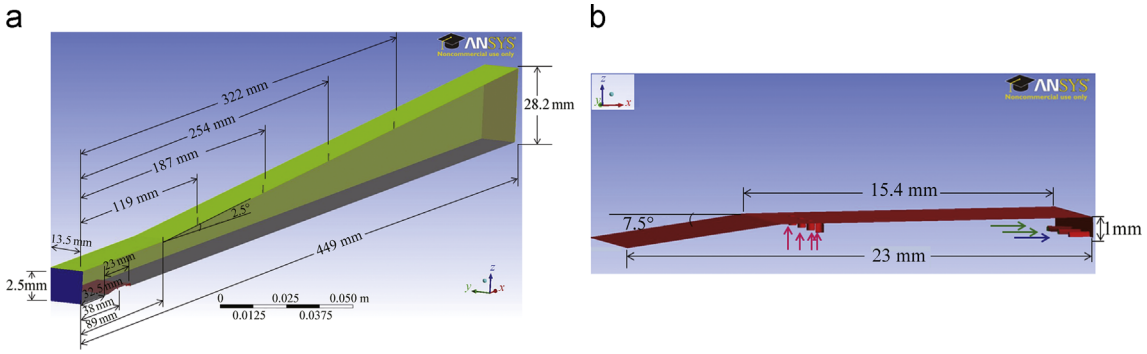

Figure 1 The dimensions of (a) the quarter combustor and (b) the wedged strut injector.

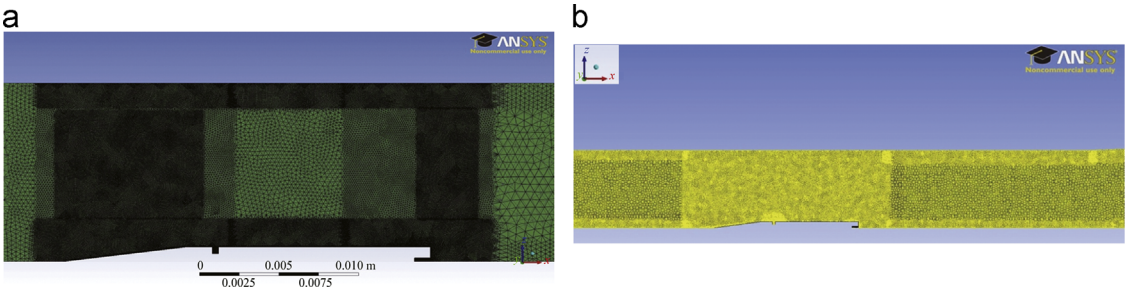

Figure 2 Grids for (a) narrow channel and (b) quarter geometries.

the narrow channel geometry contains one port for the main injection and one port for the pilot injection of H_2.

The second part of the combustor diverges with an angle of 2.5°. It involves 8 interchangeable wall injectors with a diameter of 1 mm located within the lower and upper wall at different axial positions of 119 mm, 187 mm, 254 mm and 322 mm downstream of the combustor entrance. The total length of the combustor is 449 mm.

Unstructured tetrahedral grids for the quarter geometry and the narrow channel are generated as can be seen in Figures 2(a) and (b). The meshing requirements are to minimize the computational time (CPU time) of the simulation, reduce its cost, and generate precise grid independent results. The cell size ranges between 0.4–1.4 mm. Successive refinements on the strut region and near the walls are done. The total numbers of the unstructured tetrahedral cells (TH) are 5234476 TH and 15469276 TH for the narrow channel and the quarter geometry respectively.

2.2. *Mathematical and numerical modelling*

Steady 3D simulations are carried out to calculate the flow field and turbulent mixing behaviour of H_2/Air by using Ansys CFX code. Reynolds-averaged Navier-stokes (RANS) equations are adopted in these simulations to predict the wall static pressure distribution and shock wave interactions along the combustion chamber for the case of no hydrogen injection and in the cases of single (strut) and multi-staged (strut and wall) H_2 injection. Ideal gas compressible flow is considered. The shear stress transport (SST) turbulence model with two equations k-ω model is selected because SST model accounts for the turbulent shear stress and predicts the amount of flow separation while k-ω model computes the near wall treatment for low-Reynolds number, $y+<2$. The total energy model is used for supersonic flow in a scramjet. Conservation Navier Stokes equations for the variable composition mixtures of H_2/air are solved and can be expressed as follows:

Mass conservation:

$$\frac{\partial \rho_m}{\partial t} + \frac{\partial \left(\rho_m u_m^i\right)}{\partial x^i} = 0 \tag{1}$$

$$\rho_m = \sum_{i=A,B,C,\ldots}^{N_C} Y_i \rho_i \tag{2}$$

where ρ_m is the mixture density, u_m is the mixture velocity and Y_i is the mass fraction of component i.

Species mass conservation equations:

$$\frac{\partial}{\partial t}\left(\rho_m Y_i\right) + \nabla\left(\rho_m U_i Y_i - \rho_m D_i (\nabla Y_i)\right) + S_i = 0 \tag{3}$$

$$\nabla U_i = \frac{\partial u_x}{\partial x} + \frac{\partial u_y}{\partial y} + \frac{\partial u_z}{\partial z} \tag{4}$$

$$\sum_{i=A,B,C,\ldots}^{N_C} Y_i = 1 \tag{5}$$

Momentum conservation:

$$\frac{\partial \left(\rho_m u_m^i\right)}{\partial t} + \frac{\partial \left(\rho_m u_m^j u_m^i\right)}{\partial x^j} = -\frac{\partial p}{\partial x^i} + \frac{\partial \tau_m^{ji}}{\partial x^j} + \rho_m g^i \tag{6}$$

where g is the gravity acceleration and τ_m^{ji} is the shear stress of component i in the mixture.

The total energy equation:

$$\underbrace{\frac{\partial(\rho h_{tot})}{\partial t}}_{\text{Work of pressure forces}} \underbrace{-\frac{\partial P}{\partial t}}_{\text{Convective transport}} + \underbrace{\nabla(\rho U h_{tot})}_{\text{Heat conduction}} = \underbrace{\nabla(\lambda \nabla T)}_{\text{viscous work}} + \underbrace{\nabla(U \cdot \tau)}_{\text{chemical source}} + S_E \tag{7}$$

where h_{tot} is the total enthalpy.

$$\tau = \mu\left(\nabla U + (\nabla U)^{\mathrm{T}} - \frac{2}{3}\delta\, \nabla \cdot U\right) \tag{8}$$

Turbulence model:

The transport equations of SST turbulence model based on k-ω model can be written as following:

The turbulent kinetic energy k equation:

$$\frac{\partial(\rho k)}{\partial t} - \frac{\partial}{\partial x_j}(\rho\, U_j k) = \frac{\partial}{\partial x_j}\left[\left(\mu + \frac{\mu_t}{\sigma_k}\right)\frac{\partial k}{\partial x_j}\right] + P_k - \beta' \rho k\omega + P_{kt} \tag{9}$$

The turbulent frequency ω equation:

$$\frac{\partial(\rho\omega)}{\partial t} - \frac{\partial}{\partial x_j}(\rho\, U_j \omega) = \frac{\partial}{\partial x_j}\left[\left(\mu + \frac{\mu_t}{\sigma_\omega}\right)\frac{\partial \omega}{\partial x_j}\right] + \alpha\frac{\omega}{k}P_k - \beta\rho\omega^2 + P_{\omega t} \tag{10}$$

$$\mu_t = \rho\frac{k}{\omega} \tag{11}$$

where μ_t is the turbulent viscosity and P_k is the turbulence production due to viscous and buoyancy forces.

For the SST model:

$$v_t = \frac{\alpha_1 k}{\max(\alpha_1\omega, SF)} \tag{12}$$

where v_t is the kinematic eddy viscosity.

$$v_t = \mu_t/\rho, \qquad F = \tanh(\arg^2) \tag{13}$$

where F is a blending function, $F=1$ near the surface, $F=0$ outside the boundary layer.

$$\arg = \max\left(\frac{2\sqrt{k}}{\beta'\omega y}, \frac{500v}{y^2\omega}\right) \tag{14}$$

where, y is the distance to the nearest wall.

The transported RANS equations are discretized by using the finite volume (FOV) method, where the total volume is divided into small control volume. Suitable interpolation and integration methods are used to get algebraic equations which are solved iteratively. The SST turbulence equations are coupled with the momentum equation by the implicit iterative algorithm and solved numerically by using high resolution and first order methods. The solution is considered convergent when the residuals in the solved equations become smaller than prescribed tolerance of 1×10^{-9}. Steady simulations with 10000 iterations are set to get sufficient, accurate, and precise results. The results of the solved equations give the quantitative and qualitative description of the Mach number, flow velocity field, pressure distribution, density distribution, and concentrations of the mixture components.

2.3. Initial and boundary conditions

Preheated air at a total temperature ($T_{t,\max}$) of 1000 K and a total pressure ($P_{t,\max}$) of 1 MPa is expanded through a Laval nozzle and enters the combustor at a Mach number (Ma) of 2.2. The mass flow rate of the air is 360 g/s. Subsonic hydrogen is injected through the main injector perpendicular to the free air stream with a mass flow rate of 1.5 g/s and through the pilot injector parallel to the free air stream with a mass flow rate of 90 mg/s at a temperature of 230 K. The boundary conditions at the walls of the combustor are those derived assuming no-slip condition with regards to Dirichlet condition with a fixed temperature of 310 K. Supersonic outlet conditions are applied. The mass flow rate of the hydrogen injected through the wall injector normal to the free air stream is 1 g/s. Symmetric boundary conditions are used. All computations are initialized with the state of the incoming air.

3. Results and discussion

3.1. Effects of the geometry and grid

3.1.1. Wall pressure distribution

The predicted static pressure distributions along the wall of the combustor in case of no H_2 injection, for both narrow channel (Narr. Chann.) and quarter combustion chamber (Quarter CC.) geometries, show a good agreement with the experimental pressure data as can be seen in Figure 3. Both geometries give similar results with very small differences especially in the divergent part of the combustion chamber where a highly accelerated supersonic flow exists.

Pressure peaks show the strength of the shocks and their positions. The first high pressure peak is caused by the interaction between the shock formed at the leading edge of the strut and the combustor wall. The remaining low pressure peaks further downstream are caused by impingements of multi-reflections of the initial shock generated at the leading edge of the strut. Low pressures downstream of

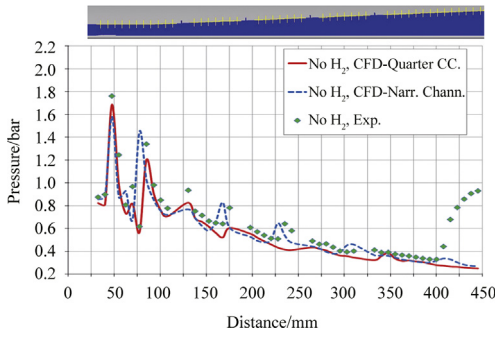

Figure 3 Static pressure distributions along the wall of the combustor experimentally and with CFD simulations in case of no H_2 injection.

the strut at 50 mm $< x <$ 75 mm are due to the expansion fans caused by the corner of the trailing edge of the strut. The expansion of the flow in the divergent part of the combustion chamber at $x > 89$ mm causes flow acceleration and pressure decrease. Therefore, the strength of the reflected shocks (pressure peaks) and the reflection angle from the combustor walls decrease. Thus, the distance between the reflected shocks increases.

Both geometries in the cases of pilot H_2 injection and main plus pilot H_2 injection also give similar pressure distributions along the wall of the combustor with very small differences, as can be seen in Figures 4(a) and (b).

Due to the finer mesh in the whole area of the narrow channel case, the predicted wall pressure values for this case are closer to the experimental data from that in the quarter geometry case, especially in the rear part of the combustion chamber at $x > 125$ mm.

The static pressure increases at the exit of the combustion chamber at $x > 390$ mm to adapt the higher external ambient pressure. This type of flow behaviour is not considered in the calculations.

Reducing the cells three times from 15 million (quarter geometry) to 5 million (narrow channel), reduces the computational time from one month to one week.

3.1.2. *Flow field visualization*

The predicted flow field — shock interactions — is illustrated by using the contour plots of density, Mach number, pressure and velocity for both the narrow channel and the quarter combustor geometries, as can be seen in Figure 5. The interaction of the shock caused by the leading edge of the strut and the expansion fans with the boundary layer at the wall leads to complex shock train along the combustion chamber with a complex supersonic flow, as shown in Figure 5.

Weak shocks are obtained in the rear part of the divergent section due to the accelerating supersonic flow, where eddies are created in the area between the centre line of the combustor and the reflected shocks – as can be seen from Mach number distribution in Figure 5(a) to enhance the turbulent H_2/air mixing efficiency. The differences in the geometry between the two cases have only a minor impact on the overall flow field. Nevertheless, small differences in density, pressure, Mach number and velocity distributions are observed.

High density and pressure values are found at the interaction points with the wall at which the boundary layer (B.L.) separates (see velocity field in Figure 5(b)) and at the interaction between the reflected shocks with the free stream and expansion waves. In contrast, these points show low Mach numbers and velocities.

3.2. *Effect of injection type*

3.2.1. *Single first stage injection (strut)*

3.2.1.1. Wall pressure distribution. A comparison of the wall static pressure distribution along of the combustor in the cases of pilot H_2 injection, which is parallel to the free stream, both pilot and main H_2 injection, which is normal to the free stream, and in the case of no H_2 injection at all can be seen in Figure 6.

The positions of the reflected shocks from the strut leading edge shock are clearly visible at $x = 85$, 130, 167, 227 and 310 mm.

The pressure values in the cases of no H_2 injection and only pilot H_2 injection parallel to the main flow are similar in form and amplitude. But there is a small increase in the amplitude and shift in the position of the pressure peaks upstream at $x > 125$ mm due to the main H_2 injection normal to the free stream flow. The position of the reflected shocks is slightly shifted upstream at $x > 125$ mm depending on the reflection angle from the combustor walls. Larger distances between the pressure peaks – caused by lower reflection angle of the shocks – lead to a wider shock structure.

The low amplitude pressure peaks at $x > 89$ mm downstream in the divergent section of the combustor correspond to the flow expansion and acceleration to high Mach numbers. Thus the strength of the reflected shocks decreases. The flow expansion is accompanied by thickening of the boundary layer. The static pressure at $x = 390$ mm

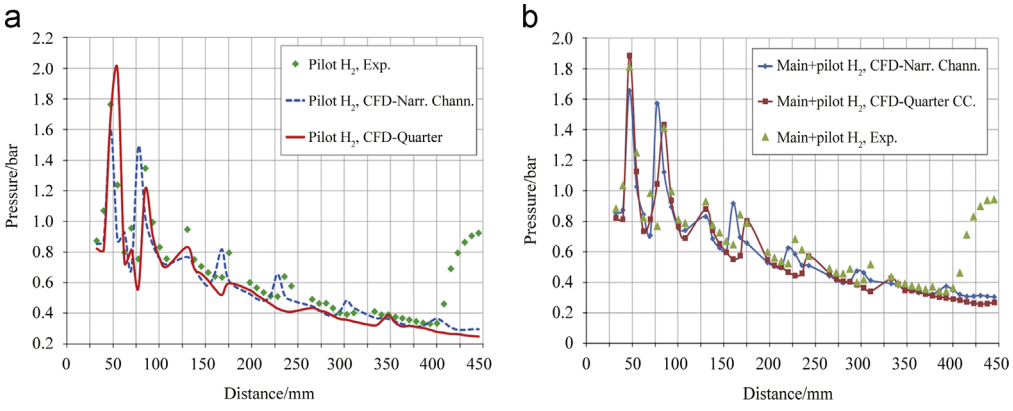

Figure 4 Static pressure distributions along the wall of the combustor experimentally and with CFD simulations for (a) pilot H_2 injection and (b) main+pilot H_2 injection.

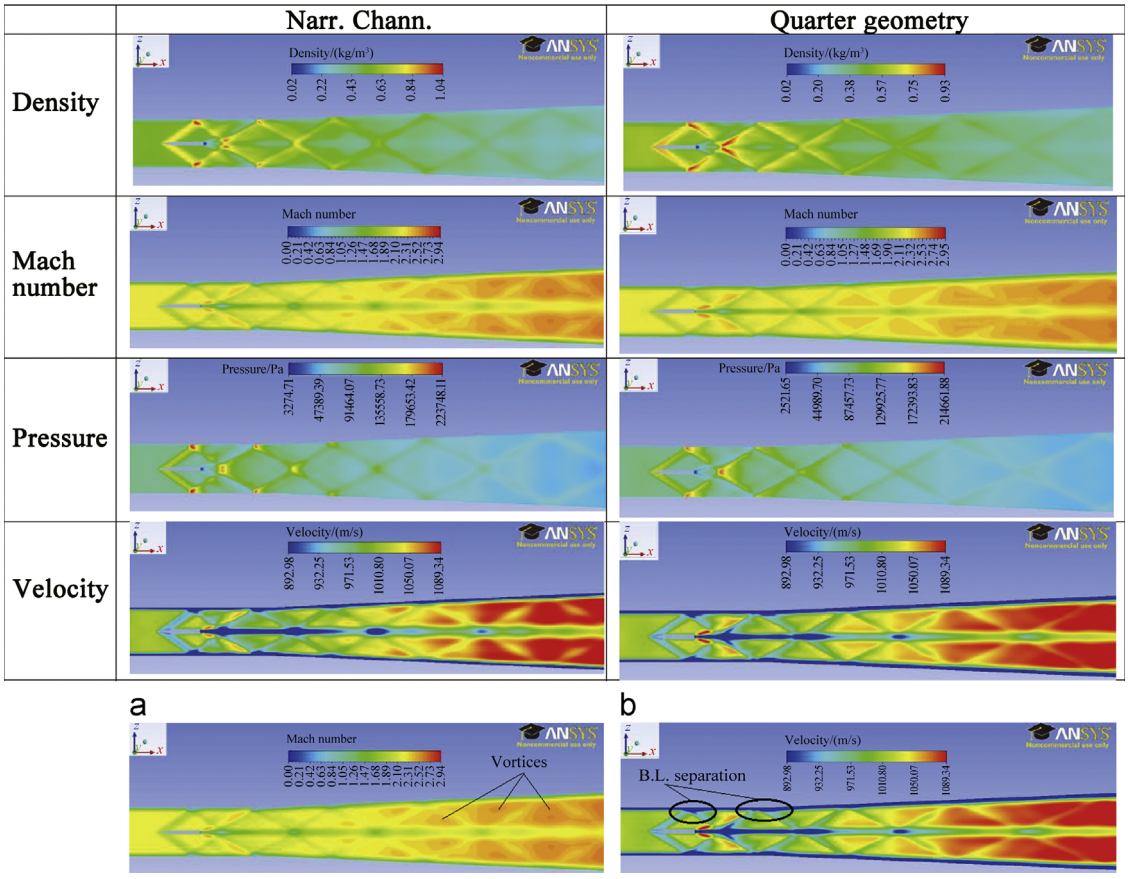

Figure 5 CFD predicted flow field by using contour plots of the density, Mach number, pressure and velocity for the narrow channel (left) and quarter geometry (right). Illustration of (a) the predicted vortices and (b) the boundary layer separation.

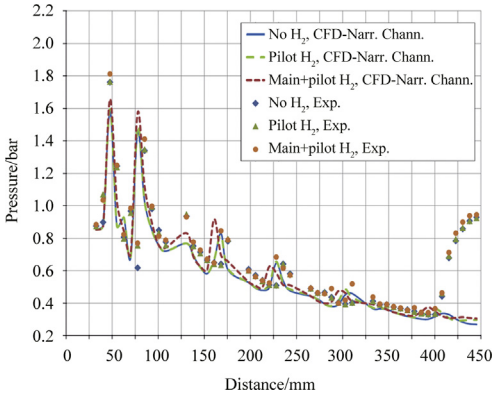

Figure 6 Static pressure distributions comparison along the wall of the combustor for no injection, pilot injection and main+pilot injection of H_2, experimentally and with CFD simulations.

adapts to the ambient pressure because it is higher than the static pressure in the combustion chamber. So, the pressure rise at the end of the chamber is caused by the back pressure as the boundary layer separates.

The calculated and measured static pressure distribution values along the wall of the combustor are in a good agreement. Similar pressure distributions with very small differences are observed.

3.2.1.2. Flow field visualization of H_2/air. The predicted flow pattern of the shock train due to the H_2 injection in the pilot and main injectors is compared with that in case of no H_2 injection, as can be seen in Figures 7(a) and (b). Shock interactions with the accelerating wake behind the wedge and their influence on the flow behaviour is illustrated by using contour plots of pressure, Mach number, velocity and density distributions.

In the case of no H_2 injection, the oblique shock with high pressure coming from the wedge tip is visible and in a good agreement with the schlieren photo in Figure 8 as well as its strength (amplitude) and position in Figure 6. The shock reflects off the upper wall of the combustor and hits the wake down the channel - because of the diverging section - forming a symmetrical shape along the combustion chamber. The boundary layer on the wedge separates and forms a shear layer between the wake and main stream flow.

Strong expansion fans with high Mach numbers are formed at the trailing edge of the strut resulting in partially curved recompression shocks, which are reflected from the combustor wall and start to interact with the rest of the flow field. The flow behind the wedge accelerates towards the centreline of the combustor. Boundary layer thickening and wall temperature increase are caused by the reflected shocks from the combustor walls. A more intense expansion fan is formed near the corner of the trailing edge of the wedge in case of no H_2 injection.

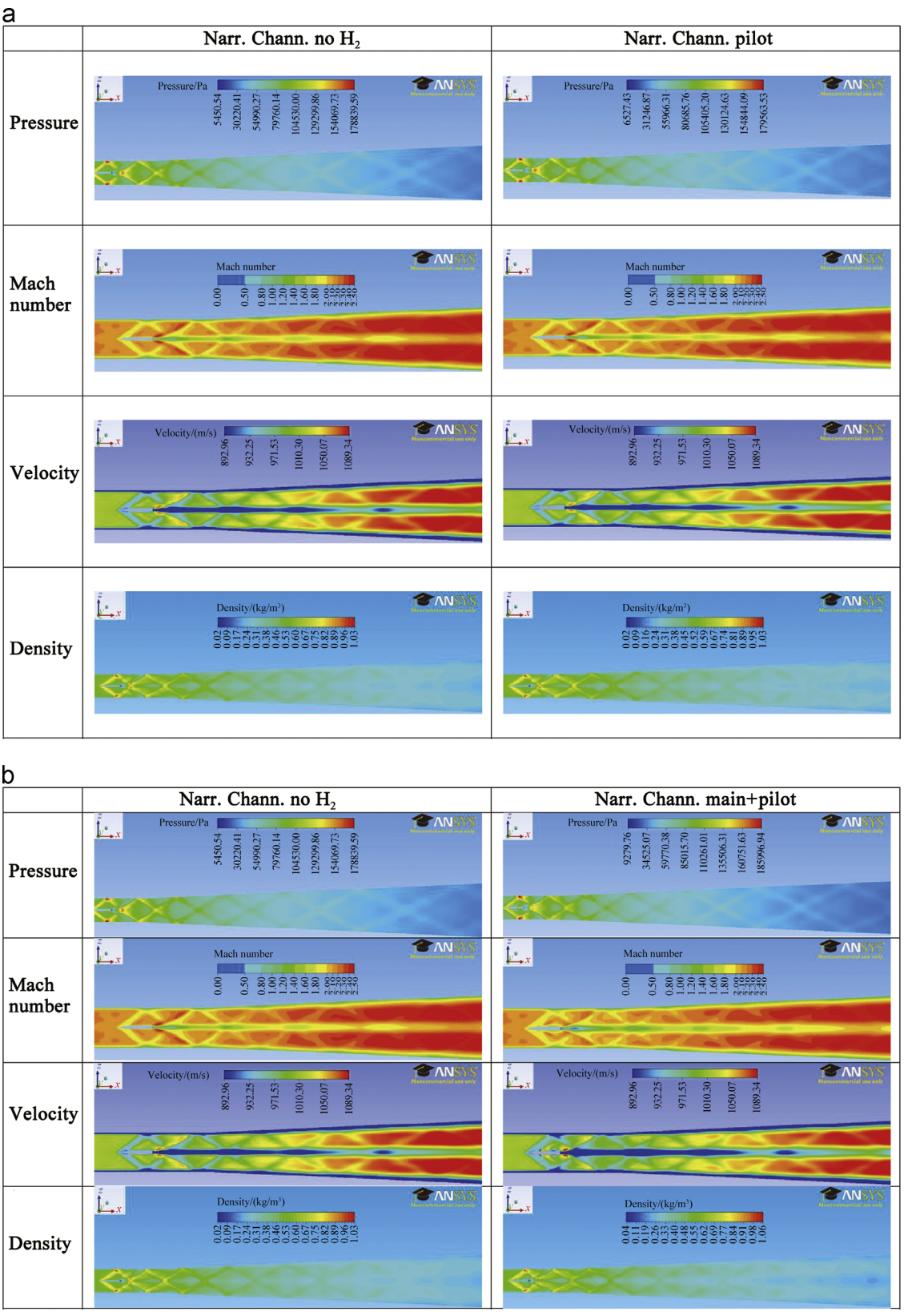

Figure 7 CFD predicted shock waves interactions for no H_2 injection (left) and (a) pilot H_2 injection (right) and (b) main+pilot H_2 injection (right) by using contour plots of the pressure, Mach number, velocity and density.

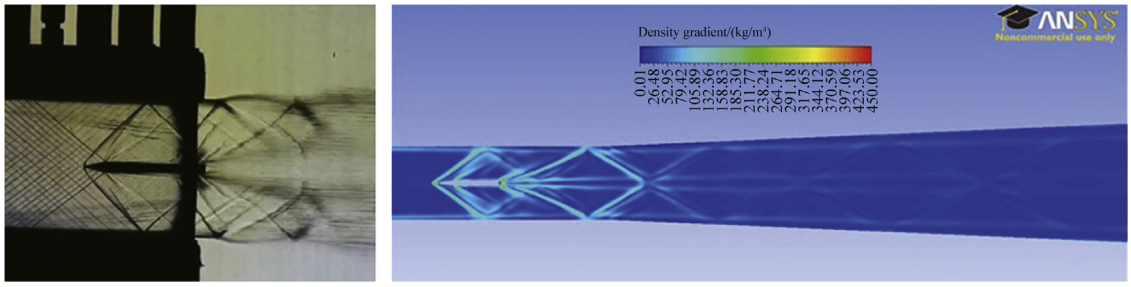

Figure 8 Shock waves interactions experimentally (left) by schlieren image and with CFD simulation (right).

The H_2 injected through the pilot parallel to the main flow is mixed with the air – without combustion – to yield a flow structure almost identical to that in the case of no H_2 injection, with only small differences. Oblique shocks are formed at the tip leading edge of the wedge, which are then reflected by the upper and lower walls before interacting with the H_2 filled subsonic wake further downstream. The boundary layers at the walls are affected by the reflected oblique shocks. Downstream of the wedge, the flow is accelerated back to supersonic speed.

The small diamond shaped circulation behind the wedge is caused by the low velocity in that region. The expansion fans at the trailing edge of the strut are weaker than those obtained from the first case of no H_2 injection. The re-compression shocks become weaker and show a less pronounced curvature than that observed in the case of no H_2 injection.

It can be seen in Figure 7(b) that the boundary layer separates on the surface of the wedge at the base and shear layers are formed due to main H_2 injection perpendicular to the main flow. A subsonic recirculation zone is formed at the base of the wedge which will help stabilize the flame in case of combustion. The recirculation zone downstream of the strut is found to be longer and wider in comparison with the cases of pilot and no H_2 injection, as can be seen from the velocity distribution in Figure 7(b) (right). This is due to the high pressure caused by the injected H_2 (lower velocity) normal to the main flow. This zone shows big changes in the velocity values between subsonic and supersonic, as can be seen from Mach number distribution in the same figure.

Better mixing of H_2 with air is obtained in the case of main H_2 injection due to the vortices formed above the wedge. This leads to a larger area of flow separation at the walls of the combustor due to the higher pressure of impingements in the walls. The angle of the reflected shocks increases when they pass through the wake flow, the width of the shocks (distance between shocks) decreases and thus the number of shocks increases, as can be seen from pressure contour plot in Figure 7(b). The large number of the reflected shocks in the rear part of the combustor yields flow acceleration and enhances the turbulent mixing.

Due to the large density gradient, the lighter H_2 exists in the shear layers between the wake and the free stream. The shear layer growth is influenced by compressibility effects. Velocity and density gradients "as well as convective Mach number" affect the compressibility and thus the formation and breakup of shock structure. Reducing the compressibility

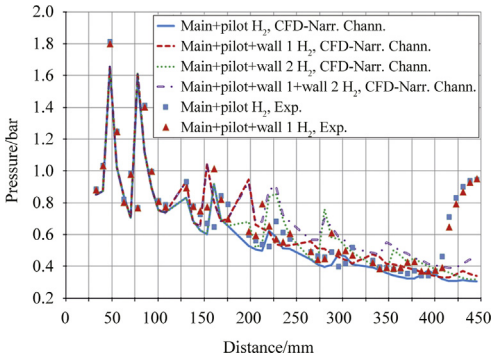

Figure 9 Wall pressure distributions for single-stage (main+pilot) and multi-stage H_2 injection through wall 1 and wall 2, experimentally and with CFD simulations.

due to the flow expansion and acceleration decreases the strength of the shear layers downstream the wedge and increases the growth rate of large scale eddies as well as the overall rate of mixing.

A qualitative comparison of experimental schlieren image (left) – based on the density gradient – of the flow and shock waves interaction and CFD predicted flow pattern (right) by using density gradient contour is shown in Figure 8. A very good agreement is obtained.

3.2.2. Multistage injection (wall injectors 1 and 2)

3.2.2.1. Wall pressure distribution. A comparison of the pressure distribution between the single-stage injection in the strut (main+pilot injectors) and multi-stage injection through wall 1 at $x = 119$ mm, wall 2 at $x = 187$ mm and wall 1 plus wall 2 is shown in Figure 9.

A good agreement is found between the experimental and the CFD predicted data. The flow path of the shock structure of the multiple reflected shocks upstream of the wall injectors at $x = 119$ mm and 187 mm for wall 1 and wall 2, respectively is unchanged. Therefore the pressure peaks are not affected upstream of the wall injection points, but they become higher and shifted upstream in the rear part of the combustor downstream of the injection points. This is due to the formation of strong bow shocks upstream of the wall injectors.

The reflected leading edge shocks, the bow shocks with different strength and angle, the reattached separated layers up and downstream of the wall injectors interact strongly together

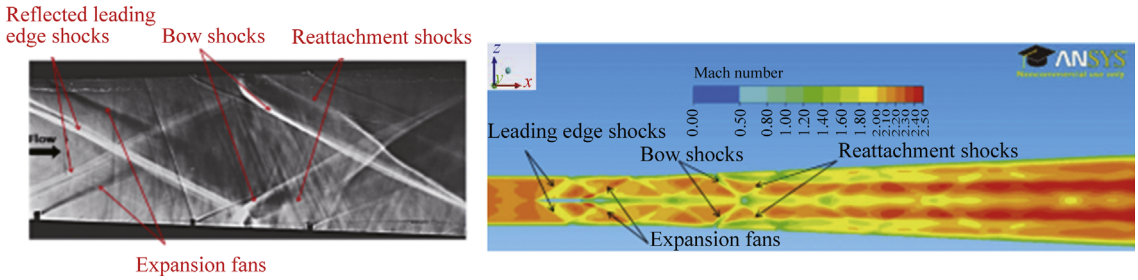

Figure 10 Schlieren image (left) and CFD predicted Mach number contour (right) for wall 1 injection.

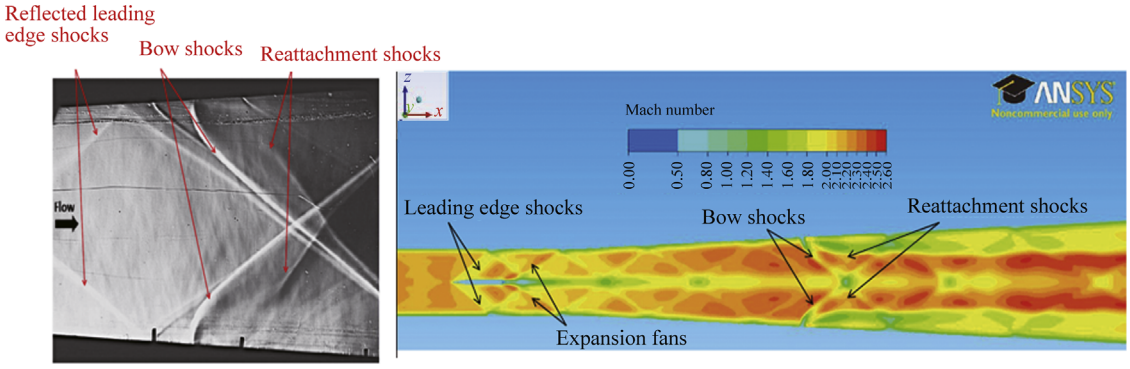

Figure 11 Schlieren image (left) and CFD predicted Mach number contour (right) for wall 2 injection.

with the wake and reflect at the combustor wall resulting in high pressure peaks next to the wall injectors at $x = 153$ mm and 223 mm for wall 1 and wall 2, respectively. These shocks are reflected several times at the combustor wall downstream of the wall injectors to get new pressure peaks with different strength and position at 175 mm $< x <$ 225 mm, 250 mm $< x <$ 275 mm and 325 mm $< x <$ 350 mm in the case of wall 1 injection and at 250 mm $< x <$ 300 mm, 350 mm $< x <$ 400 mm in the case of wall 2 injection.

The pressure rise due to wall 1 H_2 injection is higher than that due to the wall 2 H_2 injection because wall 2 injector exists in the larger area of the combustor where the interaction of the shocks is weaker and the flow is accelerated even further.

3.2.2.2. Flow field visualization: experiment and CFD simulations. The flow pattern visualized experimentally by using schlieren method and from CFD simulations for wall 1 and wall 2 H_2 injectors can be seen in Figures 10 and 11, respectively.

Schlieren pictures show the mean density gradient in the combustion chamber along the optical axis of the schlieren setup. The flow structure (bow shocks, separated boundary layer due to the wall injection, reattachment and the reflected shocks) described previously is clearly visible in Figures 10 and 11. The vortices are created at the centre line of the flow enhancing the mixing and increasing the interfacial area between H_2 and air, and thus accelerating the flow to a higher supersonic velocity as well as the combustion. The bow shock caused by wall 2 injection is weaker than that caused by wall 1 injection due to the increased cross sectional area in the rear part of the combustor, as can be seen in Figures 10 and 11.

3.2.2.3. Flow field visualization of H_2/air (wall 1). Figure 12 presents the difference between the flow pattern in case of single-stage injection (main and pilot) and multi-stage injection with wall 1.

It is clear from the pressure distribution that the shock train becomes longer due to the higher number of the reflected shocks which are generated downstream of the wall 1 injector. This leads to a further flow acceleration in the divergent part of the combustor. The strong bow shocks generated upstream of the wall injector, the reattachment shocks formed from the separated layers beyond the wall injector and the reflected ones are responsible for that behaviour which results from the high reflection angles and thus the small distances between the reflected shocks. This can be seen from Mach number and velocity contour plots which show the highly turbulent mixing region with high degree of vortex formation.

Turbulence near the wall and boundary layer separation results in better mixing with air through the formation of large eddies near the wall. Thus, lower mixture densities are obtained in the rear part of the combustion chamber, as illustrated by density contour plot in Figure 12.

Flow separations beyond the bow shock, as well as downstream recompression shock, are identified from Mach number contour plot in Figure 12.

3.2.2.4. Flow field visualization of H_2/air (wall 2). The comparison between the flow pattern in case of single-stage injection (main and pilot) and multi-stage injection with

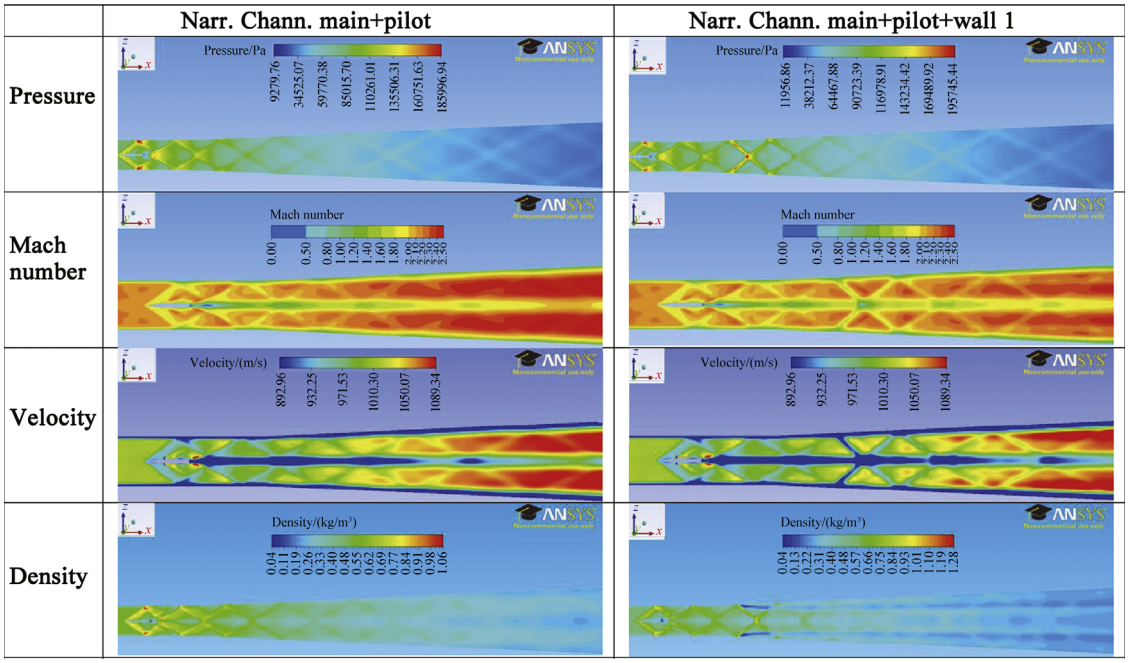

Figure 12 CFD predicted flow field visualisation for single-stage (left) and multistage H_2 injection through wall 1 by using contours of the pressure, Mach number, velocity and density.

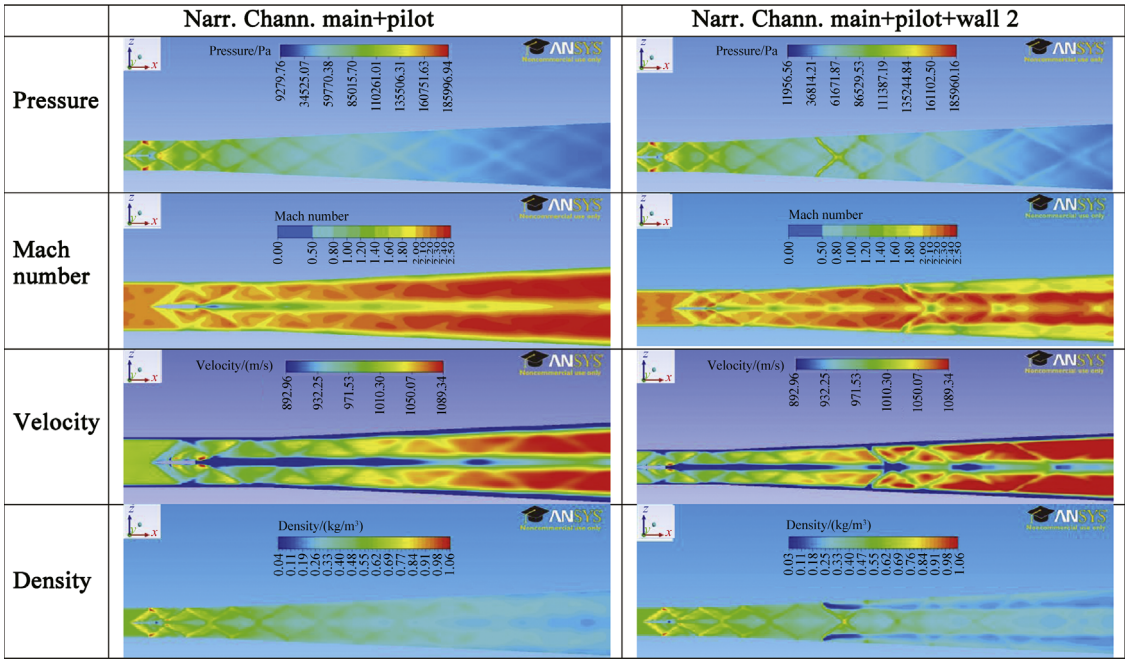

Figure 13 CFD predicted flow field visualisation for single-stage (left) and multi-stage H_2 injection through wall 2 by using contours of the pressure, Mach number, velocity and density.

wall 2 can be seen in Figure 13. Pressure contour plots show that a higher number of reflected shocks is created downstream of wall 2 injector due to the bow shock generated upstream of wall 2. Better turbulent mixing and more vortices are formed along the wall of the combustion chamber, as illustrated by Mach number contour plot. This is due to larger turbulence area and more pronounced boundary layer separation downstream of wall 2 injector. The fuel mixes with air in the subsonic separated region near the wall. The reflected shocks further downstream in the rear part of the combustor do not reach through to the wall surface because they interact with H_2 stream injected

through wall 2 injector. Therefore, the vortices are concentrated at the core downstream (centre line of the flow), where strong mixing occurs and highly accelerated flow exists.

The growth rate of the vortices is stopped by the recompression shock downstream of wall 2 injector even going to a negative growth rate, as shown by the velocity contour plot. Thus, new small scale vortices are generated into the free stream at the edge of the shear layers, as shown by the contour plot of Mach number in Figure 13.

3.2.2.5. Flow field visualization of H_2/air (wall 1+ wall 2). The case of H_2 injection in both wall injectors leads to more turbulent mixing in the centre line of the flow, as can be seen from the velocity flow field in Figure 14. The bow shock created by H_2 injection in wall 2 is weaker than that created by H_2 injection in wall 1. Thus the number of the reflected shocks beyond wall 2 injector are smaller than that in the upstream due to increasing the cross sectional area of the divergent part and decreasing the angle of the reflected shocks. Wall 1 injector yields better H_2/air mixing because it leads to a higher penetration depth in comparing with wall 2. This is due to the higher interaction wall pressures which lead to higher reflection angles and thus thinner shock structure with more number of shocks, as can be seen from the pressure field in Figure 14.

Larger area of boundary layer separation, in case of both wall 1 and wall 2 H_2 injectors is obtained. Thus, more shocks are formed in the rear part of the combustion chamber leading to more turbulent mixing near the wall.

The multi-stage wall injection widens the high pressure region near the wall due to the generated vortices and causes better H_2/air mixing. Thus wall injection will lead to a stronger combustion and wider temperature region near the wall.

3.3. Pressure losses

Three-stage injection of H_2 through the strut, wall 1 and wall 2 increases the total pressure losses in the combustor to approximately two times that obtained due to the single-stage injection of H_2 through the strut, whereas the total pressure losses due to the two-stage injections of H_2 (strut+wall 1 or strut+wall 2) are very close about 44% (see Figure 15).

As discussed before, wall injection causes higher number of shocks and thus shock interactions leading to more pressure losses in the combustor.

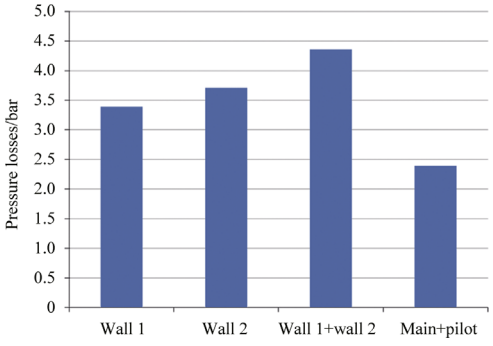

Figure 15 Total pressure losses in the combustor for different configuration of H_2 injection (strut+wall 1, strut+wall 2, strut+wall 1+wall 2 and only strut (main+pilot)).

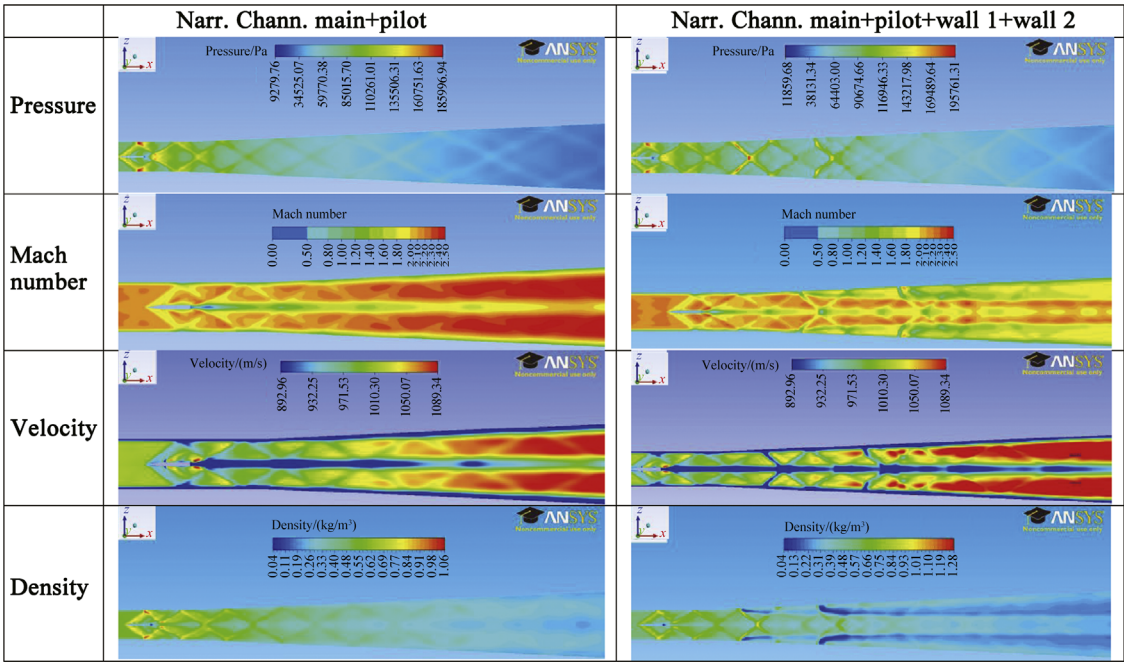

Figure 14 CFD predicted flow field visualisation for single-stage (left) and multi-stage H_2 injection through wall 1+wall 2 by using contours of the pressure, Mach number, velocity and density.

4. Conclusions and outlook

CFD simulations are able to predict the characteristics of shock waves, their flow pattern, their locations, the interactions and the physical properties of the shock layer. A good agreement is found between the CFD predicted pressures and flow fields with the experimental data. CFD predicted data from the narrow channel give similar results to the predicted data from the quarter geometry with small differences. Narrow channel geometry can be used for further CFD simulations of the single and multi-stage supersonic combustion of H_2 with combustion to reduce the computational time.

Wall injectors enhance the turbulent H_2/air mixing by eddy formation and thus enable stronger combustion. The location of the wall injector plays a key role in the H_2/air mixing efficiency.

The anticipated future work is to make CFD simulations for the multi-stage interchangeable wall injectors three and four in case of no combustion. Steady and transient CFD simulations of single and multi-stage H_2 injection "including the combustion reaction" will be done by testing different combustion models and reaction kinetics. The total pressure losses in the case of cold flow will be compared with pressure losses and heat release in the case of combustion to determine the best injection condition at which minimum pressure losses and maximum heat release can be obtained.

Acknowledgements

The authors would like to thank the German research foundation (DFG) for their financial support for this work in the framework of the research training group GRK 1095.

References

[1] D. G. Andrew, J. E. Andrews, Designing for the future space transportation missions, in: The 37th Joint Propulsion Conference and Exhibit, AIAA-2001-3964, 2001.
[2] D. Maier, S. Kirstein, T. Fuhrmann, S.R. Denis, A. Hupfer, H.P. Kau, Scramjet research activities at the institute of flight propulsion of the Techniche Unversitaet Muenchen, in: The 6th European Symposium on Aerothermodynamics for Space Vehicles, Versailles, France, 3–6, November, 2008.
[3] K.M. Pandey, T. Sivasakthviel, CFD analysis of mixing and combustion of a scramjet combustor with a planer strut injector, International Journal of Environmental Science and Development 2 (2011) 102–108.
[4] K.M. Pandey, T. Sivasakthviel, CFD analysis of hydrogen fuelled mixture in scramjet combustor with a strut injector by using fluent software, International Journal of Engineering and Technology 3 (2011) 109–115.
[5] P. Gerlinger, P. Stoll, M. Kindler, C.F. Schneider, M. Aigner, Numerical investigation of mixing and combustion enhancement in supersonic combustors by strut induced stream vorticity, Aerospace Science and Technology 12 (2008) 159–168.
[6] J.H. Kim, Y. Yoon, I.S. Jeung, H. Huh, J.Y. Choi, Numerical study of mixing enhancement by shock waves in model scramjet engine, AIAA Journal 41 (2003) 1074–1080.
[7] T. Sunami, A. Murakami, M. Nishioka, Mixing and combustion control strategies for efficient scramjet operation in wide range of flight Mach numbers, AIAA-2002-5116, 2002.
[8] E. Fernando, S. Menon, Mixing enhancement in compressible mixing layers: an experimental study, AIAA Journal 31 (1993) 278–285.
[9] A. Shigeru, H. Arinur, M. Shingo, I. Kei, Yasuhiro, Fundamental study of supersonic combustion in pure air flow with use of shock tunnel, Acta Astronautica 57 (2005) 384–389.
[10] K. Kumaran, V. Babu, Investigation of the effect of chemistry models on the numerical predictions of the supersonic combustion of hydrogen, Combustion and Flame 156 (2009) 826–841.
[11] H. Lingyun, B. Weigand, M. Banica, Effects of staged injection on supersonic mixing and combustion, Chinese Journal of Aeronautics 24 (2011) 584–589.
[12] K.M. Pandey, B.K. Azad, S.P. Sahu, M. Prajapati, Computational analysis of mixing in Strut based combustion at air inlet Mach number 2, International Journal of Environmental Science and Development 2 (2011) 73–80.
[13] D.W. Bogdanoff, Advanced injection and mixing techniques for scramjet combustors, Journal of Propulsion and Power 10 (1994) 183–190.
[14] K.M. Pandey, T. Sivasakthviel, Recent advances in scramjet fuel injection - a review, International Journal of Chemical Engineering and Applications 1 (2010) 294–301.
[15] J.P. Drummond, in: Enhancement of mixing and reaction in high speed combustor flow fields, International Colloquium on Advanced Computation and Analysis of Combustion, Moscow, Russia, 12-15 May (1997) 1-14.
[16] G.L. Brown, A. Roshko, On density effects and large structure in turbulent mixing layers, J. Fluid Mech. 64 (1974) 775–816.
[17] D. Papamosschou, A. Roshko, Observations of supersonic free shear layers, AIAA-1986-162, 1986.
[18] D. Papamosschou, A. Roshko, The compressibility turbulent shear layer: an experimental study, J. Fluid Mech. 197 (1988) 453–477.
[19] D.W. Bogdanoff, Compressibility effects in turbulent shear layers, AIAA Journal 21 (1983) (962-927).
[20] C. Gruenig, F. Mayinger, Supersonic combustion of kerosene/H_2 mixtures in a model scramjet combustor, Institute for Thermodynamics, Technical University Munich, Germany, 2005.
[21] M. Gurtner, Experimentelle untersuchung zur mehrstufigen verbrennung in einer ueberschallbrennkammer, Diploma work, Institute of Flight and Propulsion (LFA), Technical University Munich, Germany, 2011.